Effective doses of dental cone beam computed tomography: effect of 360-degree versus 180-degree rotation angles

Sunil Mutalik, BDS, MDS,[a] Aditya Tadinada, DDS, MDSc,[b] Marco R. Molina, MD,[c] Andrés Sinisterra, BA,[d] and Alan Lurie, DDS, PhD[b]

Objectives. The aims of this study were to compare radiation absorbed dose (AD) and effective dose (ED) to tissues from cone beam computed tomography (CBCT) scans with 360-degree versus 180-degree rotations with use of different fields of view (FOV), to compare EDs calculated from measured ADs versus dose area product (DAP) values, and to compare doses to the lens of the eye (LOE) from different scan parameters.

Study Design. ADs for each protocol were measured in tissues, including the LOE, by using an anthropometric phantom. EDs were calculated on the basis of dosimetry (EDm) and DAP values (EDd). Dose differences were determined with analysis of variance (ANOVA).

Results. ADs and EDs were substantially lower for 180-degree rotation scans compared with 360-degree rotation scans ($P < .01$). Remainder tissues had the greatest effect on effective dose for most FOVs. Doses were generally lower with small FOVs compared with large FOVs. Most EDm values were lower than EDd values in large FOVs but higher in small FOVs. Differences in EDm and EDd were variable and unpredictable. LOE doses were smaller with the 180-degree scans and smaller FOVs.

Conclusions. Radiation doses were generally lower with 180-degree rotation scans and smaller FOVs. These parameters should be used for CBCT acquisitions, whenever possible, and should be made available in all units. (Oral Surg Oral Med Oral Pathol Oral Radiol 2020;130:433−446)

Before the advent of the use of cone beam computed tomography (CBCT) in dentistry in the 1990s, multidetector computed tomography (MDCT) was the mainstay in most oral and maxillofacial radiology advanced imaging procedures. The effective dose (ED) for maxillofacial MDCT examinations ranged from 474 to 1160 microsieverts (μSv).[1] EDs for earlier CBCT models were comparable with the MDCT maxillofacial examinations.[2] However, EDs from current CBCT units can be as low as 5 μSv for a small field of view (FOV) and as high as 1073 μSv for large FOV scans.[3]

Ever since the discovery of x-rays, the risk from diagnostic radiation exposure has been debated in the literature.[3] The cancer risk from MDCT examinations alone may be as high as 1.5% to 2% of all cancers in the United States.[4] Studies on the survivors of atomic bomb explosions and those on other radiation-exposed cohorts have shown that there is likely no lower limit for a "safe radiation dose" for solid tumors and for leukemia. In spite of the uncertainties in risk estimation from low doses of x-radiation, the linear non-threshold (LNT) model for radiation carcinogenesis at low doses continues to be prudent.[5,6] Increased numbers of CBCT examinations have elevated the amount of cumulative dose to those undergoing these procedures. Compared with adults, the pediatric and adolescent populations are at greater risk because of their active cellular growth and organ development,[7] their longer projected lifespan, and their 4 to 10 times higher sensitivity to radiation-induced cancers.[4]

Thus, in consideration of the ALARA principle of keeping radiation exposure "As Low As Reasonably Achievable," it is important to minimize CBCT doses while ensuring the diagnostic efficacy of the examinations. Early efforts to reduce exposure during CBCT examinations involved the use of various radiation protection devices.[8,9] Operators now can manipulate exposure parameters, such as kilovoltage peak (kVp or tube voltage), milliamperage (mA or tube current), exposure time and voxel size,[10-13] to reduce dose and yet maintain image quality. Significant dose reduction also can be achieved by reducing the FOV (especially the height of the field) for a given scan.[14]

Statement of Clinical Relevance

This study showed significant radiation dose reductions in cone beam computed tomography (CBCT) acquisitions with 180-degree, instead of 360-degree, rotation arcs and smaller fields of view. CBCT machine dose area products are unreliable for dose and risk determinations.

[a]Sessional Faculty, University of Manitoba, Gerald Niznick College of Dentistry, Winnipeg, MB, Canada.
[b]Section of Oral & Maxillofacial Radiology, University of Connecticut School of Dental Medicine, Farmington, Connecticut, USA.
[c]Department of Diagnostic Imaging, University of Connecticut School of Medicine, Farmigton, Connecticut, USA.
[d]Section of Oral and Maxillofacial Radiology, University of Connecticut, School of Dental Medicine, Farmington, CT, USA.
9 July 2019; 10 April 2020
Published by Elsevier Inc.
2212-4403/$-see front matter
https://doi.org/10.1016/j.oooo.2020.04.008

Some CBCT scanners offer a choice of rotation angle.[13] Although most CBCT units have a single rotation angle of 360 degrees (full-rotation) around the patient,[13] some also allow smaller rotation angles of 180 degrees (half-rotation) or 220 degrees.[13] Studies have revealed as much as a 50% dose reduction with smaller rotation angles compared with 360-degree rotation angles for the same FOV.[14,15] Although there were concerns that the reduced rotation angle would compromise the quality of the reconstructed images, several laboratory studies using 180-degree rotation angles have shown diagnostic efficacy comparable with that of 360-degree scans.[16-20] Half-rotation scans are gaining importance in CBCT examinations, especially in children, because of the short scan time and the reduced dose.[14]

Phantom dosimetry is a widely used method to determine radiation doses absorbed by various specific tissues throughout the body. These measurements can subsequently be used to calculate equivalent doses and effective doses.[21] Phantom dosimetry is a tedious and time-consuming procedure. Manufacturers of MDCT and CBCT machines provide dose area product (DAP) values as a part of their dose display for all procedures. Studies have been done to determine a conversion coefficient to calculate ED from DAP.[3,22]

The primary objective of our study was to compare dosimetry (absorbed doses) and effective doses of 360-degree versus 180-degree rotations with different FOVs. We also compared the EDs calculated with measured absorbed doses from phantom dosimetry versus the DAP values displayed on the CBCT unit console, using 360-degree versus 180-degree rotation arcs.

There has been much recent debate on the sensitivity of the lens of the eye (LOE) to radiation cataractogenesis.[6,8,14] Thus, even though the dose to the LOE does not contribute to effective dose calculations, in this study, the impact of the rotation angle and FOVs on absorbed dose to the LOE was calculated and discussed as a separate but related entity throughout the text.

MATERIALS AND METHODS

The name of the machine is 3-D Accuitomo 170 CBCT Scanner. (J. Morita, Kyoto, Japan). The unit provides a range of exposure protocols and settings. All exposures were performed at 90 kVp and 7 mA, with exposure times for 360-degree (full-rotation) and 180-degree (half-rotation) scans of 17.5 and 9 seconds, respectively, according to the manufacturer's recommended settings. The FOV sizes and positions used in the study are shown in Table I.

Dose measurements were carried out on a RANDO anthropometric phantom (Nuclear Associates, Hicksville, NY), specially modified for dosimetry studies in oral and maxillofacial imaging. The phantom consists of 36 levels. Eight of the uppermost 10 levels (#2 through #9) constituting the head and neck region were used in the present study. These phantom levels consisted of detailed 3-D anthropomorphic anatomy of the human body. The embedded adult male skull contains both cortical and trabecular elements. The phantom used in this project had been prepared to receive position-indicating devices in a previous study, including slots for rectangular collimating devices and a large opening at level 6 representing the oral cavity (Figure 1).

InLight® nanoDot™ dosimeters (Landauer, Glenwood, IL) were used for radiation absorbed dose (AD) measurements. The system uses optically stimulated luminescence (OSL) technology to perform dosimetry. Each OSL nanoDot is a plastic disk infused with aluminum oxide impregnated with carbon (Al_2O_3:C). These dosimeters are commercially available and come completely annealed. The lattice imperfections created by the carbon atoms trap the electrons released by ionizing radiation. The captured energy is released as light when the dosimeters are scanned with 540-nm light from a diode. Because of the energy response of the Al_2O_3:C detector element, the photon output varies with energy for a given dose. Therefore, the microStar reader (Landauer) was calibrated to a set of reference conditions from which additional conversion factors

Table I. Exposure protocols

Field of view size (mm)	*Position*	*360-degree and 180-degree rotation*
170 × 120	Craniofacial structures including soft tissue profile of the nose and chin, both jaws, sinonasal complex, and cervical spine	Yes
140 × 100	Both jaws, sinonasal complex, c-spine	Yes
100 × 100	Both jaws	Yes
80 × 80	Both jaws	Yes
60 × 60	Anterior maxilla	Yes
60 × 60	Right maxillary molar	Yes
60 × 60	Right mandibular molar	Yes
40 × 40	Anterior maxilla	Yes
40 × 40	Right maxillary molar	Yes
40 × 40	Right mandibular molar	Yes

Figure 1. Left lateral (L) and anterior (R) views of the RANDO phantom used in this study. An adult male human skull is embedded in the tissue-equivalent material. The horizontal lines are the levels, numbered on the left, which were separated for placement of the optically stimulated luminescence (OSL) dosimeters in the appropriate tissue locations.

were applied. The conversion factor for the energy ranges produced at 90 kVp in this study was 1.12.

The 30 phantom sites measured in this study are listed in Table II. The sites were selected to include those used in prior CBCT dosimetry studies by Ludlow et al.[3] More sites were added to include the tissues used in the International Commission on Radiologic Protection (ICRP) determination of ED in 2007.[23] One dosimeter was placed in each anatomic site (Figure 2); the exact anatomic location of each site is shown in Table II. The AD recorded for each dosimeter was the average of 3 exposures for each large FOV (170×120 mm, 140×100 mm, 100×100 mm, and 80×80 mm) and 8 exposures for each small FOV (60×60 and 40×40 mm) to achieve more reliable measurements of radiation doses. The smaller FOVs required more exposure repetitions because more dosimeters were outside the field of direct exposure and absorbed only small quantities of scatter radiation. The decision on the number of exposures and rotation angles for each FOV was based on our own pilot study and on a prior investigation by Ludlow et al.[7] For every scan, a scout view was acquired. Total doses recorded by the OSL dosimetry readers were divided by the number of exposures to determine the AD per examination for each dosimeter.

Doses recorded by OSL dosimeters at different positions in a tissue or organ were averaged to obtain the average AD in micrograys (μGy). The AD to the eye was calculated as the average of the summed doses to the ipsilateral LOE and to the orbit. The products of these values and the fractions of a tissue or organ irradiated (adopted from Ludlow et al.[7]; Table III) were used to calculate the radiation weighted dose or equivalent dose (H_T) in μSv.

H_T, the equivalent dose to different tissues, was calculated as follows:

$$H_T = (W_R)(F)(AD)$$

where

H_T = equivalent dose

W_R = radiation weighting factor = 1 for x-rays

F = fraction of irradiated tissue (from Table III)

AD = average absorbed dose

EDm, the effective dose in μSv based on OSL measurements, was calculated as follows:

$$EDm = \sum (W_T)(H_T)$$

where

W_T = tissue weighting factor that represents the relative contribution of that organ or tissue to the risk (Table IV)

H_T = equivalent dose

The tissue weighting factors that were used to calculate EDm (see Table IV) were published by the International Commission on Radiologic Protection in 2007 (ICRP Publication No. 103).[23]

EDd, the effective dose in μSv based on the displayed DAP values multiplied by a conversion coefficient, was calculated as follows. We adopted the conversion formula suggested in previous studies,[22,24] taking into consideration the tube voltage value.

$$EDd = (0.001453)(kV) + (0.0118)(PKA)$$

where

kV = tube voltage

PKA = peak kerma area or the displayed DAP

The data for absorbed, equivalent, and effective doses obtained from the different protocols were entered in the SPSS statistical software program (SPSS Inc., Chicago, IL). Standard deviations and variances for average absorbed doses of individual dosimeter readings were calculated. Variance was expressed in percentages. The differences between absorbed doses, between effective doses, between effective doses calculated from dosimeters (EDm) versus effective doses calculated from DAPs (EDd), and between doses to the LOE were calculated for 360-degree and 180-degree scan protocols and for 10 different FOVs. The differences between the EDm values obtained from tissue-weighting factors and the EDd values obtained from the DAP were expressed as percentage differences. The differences in the doses were expressed as percentage differences between the 2 rotation protocols. The differences between EDm for half-rotation and full-rotation scans were analyzed by using analysis of variance (ANOVA). The alpha value was set a priori at 0.01.

RESULTS

The average absorbed doses for individual dosimeters are shown in Table V, which also shows the standard deviations and variances for individual dosimeter

Table II. Locations of dosimeters

Phantom location	*OSL ID*	*Level in phantom*	*Anatomic description*
Calvarium anterior	1	2	In the diploic space of the frontal bone immediately above the crista galli
Calvarium left	2	2	In the diploic space of the left parietal bone (in the maximum convexity of the bone)
Calvarium posterior	3	2	In the diploic space of the occipital bone immediately above the occipital protuberance
Midbrain*	4	3	In the center of the brain, 2 inches from the parietal bones and 2.5 inches from the occipital condyle and the crista galli of the ethmoid bone
Pituitary	5	3	In the base of the pituitary fossa posterior to the optic chiasm
Right orbit*	6	4	Anterolateral wall of the right orbit immediately medial to the cortical wall, flush with the roof of the orbit
Left orbit*	7	4	Anterolateral wall of the left orbit immediately medial to the cortical wall, flush with the roof of the orbit
Lens of right eye	8	3	Surface of the eye in the center of the right eye, 0.5 inch from the medial and lateral canthus of the eye
Lens of left eye	9	3	Surface of the eye in the center of the left eye, 0.5 inch from the medial and lateral canthus of the eye
Right cheek	10	5	Skin surface of the cheek, 0.5 inch below the zygomatic buttress
Nasal cavity*	11	5	Lateral wall of the inferior meatus immediately below the inferior concha
Nasopharyngeal mucosa*	12	6	In the posterior midline, 1.5 inches anterior to the cervical spine below the level of the body of the mandible
Right parotid	13	6	Lateral to the ramus of the mandible, 0.5 inch medial to the skin surface
Left parotid	14	6	Lateral to the ramus of the mandible, 0.5 inch medial to the skin surface
Right ramus	15	6	Between the two cortical plates in the marrow space
Left ramus	16	6	Between the two cortical plates in the marrow space
Tongue	17	6	1 inch posterior to the crowns of the mandibular incisor teeth in the midline
Center cervical spine	18	6	In the center of the arch of the C3 vertebra
Left back of neck	19	7	Left to the posterior vertical center of slice 7
Right mandibular body	20	7	Between the two cortical plates of the right mandibular body in the area of the premolar teeth
Left mandibular body	21	7	Between the two cortical plates of the left mandibular body
Right submandibular gland	22	8	Medial and immediately below the body of the mandible below the right molar teeth
Left submandibular gland	23	8	Medial and immediately below the body of the mandible below the left molar teeth
Left sublingual gland	24	8	Center of the line joining the center of the left submandibular gland and genial tubercles
Right sublingual gland	25	8	Center of the line joining the center of the right submandibular gland and the genial tubercles
Midline thyroid	26	9	1 inch from the skin surface in the anterior midline
Thyroid surface—left	27	9	On the skin surface in the anterior midline, slice 9
Esophagus	28	9	Inferior surface of slice 9, 2 inches anterior to the cervical vertebrae
Trachea	29	9	In the midline, 1 inch posterior to the thyroid gland
Spinal canal	30	9	Center of the spinal canal of the C6 vertebra
Remainder Tissues†			
Oral mucosa	12, 13, 14, 17, 22-25	6, 8	The tissues of the salivary glands, tongue, and nasopharyngeal mucosa.
Lymph nodes	13, 14, 22-25	6, 8	The areas of the parotid, sublingual, and submandibular salivary glands representing the buccal and submandibular group of lymph nodes
Muscle	6, 7, 18, 24, 25, 28	4, 6, 8, 9	The orbit, center of the cervical spine, esophagus, and sublingual salivary glands, representing the muscles in the orbit, around the cervical spine, esophagus, and floor of the mouth
Extrathoracic airway	11, 12, 13, 14, 22-25, 29	6, 8	The extra-thoracic airway, viz. nasal cavity, nasopharyngeal mucosa, trachea; and the areas of the parotid, submandibular, and sublingual salivary glands. These areas represent the airway from the nasal cavity to the trachea in the head and neck.

OSL ID, Optically stimulated luminescence dosimeter identification number.
*Dosimeter positions and tissues are different from those of Ludlow et al.[3]
†Remainder tissues are the 14 most radiation-sensitive tissues that do not have explicit tissue weighting factors. These tissues are the oral mucosa, lymph nodes, muscle, extrathoracic (ET) airway, adrenal glands, gall bladder, heart, kidneys, pancreas, prostate (males), small intestine, spleen, thymus, and uterus/cervix (females). Hence the dose to remainder tissues is calculated as the average of 14 tissues. They are given a group weighting factor of 0.12.

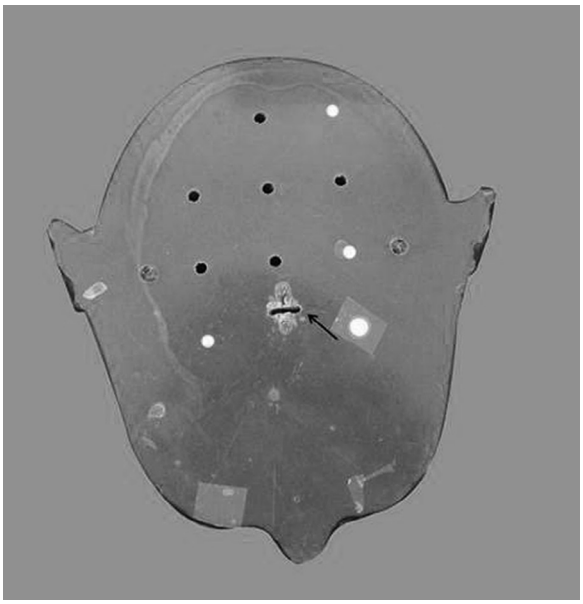

Figure 2. Axial view of the upper surface of one of the RANDO levels. The arrow indicates the nasopharynx. The holes and plugs (white) are pre-drilled holes for various types of dosimeters. The embedded skull can be seen on the right side of the level.

Table III. Fractions of the tissues or organs irradiated

Tissues/organs	*Fractions*
Bone marrow	16.5%
Mandible	1.3%
Calvarium	11.8%
Cervical spine	3.4%
Esophagus	10%
Thyroid	100%
Skin	5%
Bone surface*	16.5%
Mandible	1.3%
Calvarium	11.8%
Cervical spine	3.4%
Salivary glands	100%
Parotid	100%
Submandibular	100%
Sublingual	100%
Brain	100%
Eyes	100%
Remainder	
Oral mucosa	100%
Lymph nodes	5%
Muscle	5%
Extrathoracic airway	100%

Adapted from Ludlow et al.[7]

*Bone surface dose (BSD) was calculated as BSD = bone marrow dose × bone/muscle mass. Energy Absorption Coefficient Ratio (MEACR) (Ludlow et al.[13]). MEACR = −0.0618 × 2/3 kV peak employed (90 kV) + 6.9406, based on the equation correction for bone at 90 kV peak of 3.21 (Ludlow et al.[7]).

Table IV. International Commission on Radiologic Protection and Measurement (ICRP) 2007 tissue weighting factors (W_T)

Tissue	*ICRP 2007 W_T*
Bone marrow	0.12
Thyroid	0.04
Esophagus	0.04
Skin	0.01
Bone surface	0.01
Salivary glands	0.01
Brain	0.01
Remainder*	0.12

*Oral mucosa, lymph nodes, muscles, extrathoracic airway.

doses. The variance percentages ranged from 0.7% (left sublingual gland in the 140 × 100 full-rotation scans) to 99.2% (pituitary gland in the 40 × 40 maxillary anterior half-rotation scans). The variance was higher (> 50%) for dosimeters outside the FOV and for surface dosimeters.

Comparisons of absorbed doses between 360-degree and 180-degree scans

The majority of ADs were substantially lower in the 180-degree scans compared with the 360 -degree scans across all FOVs (see Table V; Figure 3). The highest percentage reduction, from 13.0 to 0.5 μGy (96.1%), was for the thyroid gland in the anterior maxilla area of the 40 × 40 FOV scans. The bone marrow and bone surface doses for the anterior maxilla area of the 40 × 40 FOV scans had the least reduction (9.3%) between the 2 scan protocols. The ADs for 180-degree scans were higher compared with those for the 360-degree scans for brain tissue in the anterior maxilla area of the 40 × 40 FOV scans and for the esophagus, skin, salivary gland, and brain tissue in the right maxilla molar area of the 40 × 40 FOV scans.

The contributions of individual tissues to EDm are shown in Table VI. The highest contributions were from the remainder tissues for all protocols except the right maxillary molar area of the 40 × 40 FOV 180-degree scan, where the contribution from the remainder was 19.5 μSv but the contribution from the salivary glands was 24.3 μSv. The second highest contributions came from the salivary glands for all FOVs except the 140 × 100 FOV 360-degree scan, the 100 × 100 FOV 180-degree scan, and the right mandibular molar area of the 40 × 40 360-degree scan, where doses to the thyroid glands exceeded those to the salivary glands.

Comparison of EDm between 360-degree and 180-degree scans

The measured EDm for different scan protocols are shown in Table VI and Figure 4. The EDm values for

Table V. Average absorbed doses (μGy), standard deviations (SDs), and variances (expressed in percentage) for the individual dosimeter readings

	170 × 120 A			*170 × 120 B*			*140 × 100 A*			*140 × 100 B*			*100 × 100 A*			*100 × 100 B*			*80 × 80 A*			*80 × 80 B*			*60 × 60 Anterior maxilla A*			*60 × 60 Anterior maxilla B*		
	Avg	*SD*	*Var*	*Avg*	*SD*	*Var*	*Avg*	*SD*	*Var*	*Avg*	*SD*	*Var*	*Avg*	*SD*	*Var*	*Avg*	*SD*	*Var*	*Avg*	*SD*	*Var*	*Avg*	*SD*	*Var*	*Avg*	*SD*	*Var*	*Avg*	*SD*	*Var*
Calvarium anterior	0.7	0.0	6.2	0.3	0.0	11.0	0.4	0.1	22.6	0.1	0.0	13.1	0.3	0.0	10.3	0.1	0.0	24.2	0.3	0.2	69.9	0.1	0.0	38.7	0.2	0.1	82.4	0.1	0.0	23.4
Calvarium left	0.9	0.2	22.4	0.5	0.1	19.2	0.4	0.0	3.5	0.4	0.1	34.3	0.3	0.1	37.5	0.1	0.0	17.9	0.3	0.1	20.6	0.2	0.2	83.2	0.1	0.1	76.0	0.1	0.0	85.9
Calvarium posterior	0.6	0.1	15.4	0.5	0.1	15.7	0.3	0.1	18.7	0.2	0.1	55.6	0.4	0.1	30.6	0.2	0.0	14.4	0.4	0.1	14.1	0.2	0.1	91.1	0.1	0.1	87.9	0.1	0.0	26.7
Midbrain	3.8	0.1	1.4	1.7	0.4	23.4	1.3	0.2	14.2	0.3	0.1	30.7	1.7	0.1	5.3	0.2	0.2	67.5	0.4	0.1	34.5	0.2	0.2	97.1	0.4	0.4	84.2	0.2	0.0	4.8
Pituitary	4.1	0.8	19.1	1.8	0.2	12.4	1.7	0.3	18.5	0.8	0.4	56.2	2.9	0.8	29.2	0.7	0.2	30.2	0.4	0.3	62.1	0.4	0.4	87.5	1.6	0.1	5.2	0.2	0.0	4.4
Right orbit	8.1	1.4	17.7	1.1	0.6	53.4	5.8	0.3	4.8	1.3	0.2	16.2	5.6	3.7	66.5	1.9	0.4	18.7	0.2	0.0	4.4	0.6	0.5	83.9	4.0	1.2	29.5	2.5	1.7	69.2
Left orbit	9.8	1.4	14.2	1.1	0.5	45.9	5.8	0.3	4.9	1.3	0.3	24.9	5.4	2.2	39.7	2.5	1.0	38.9	0.5	0.1	22.5	0.9	0.7	80.8	5.0	2.0	40.0	1.7	1.0	58.2
Lens of right eye	8.1	1.7	20.7	1.4	0.4	25.7	1.5	0.3	20.3	0.3	0.1	28.1	1.6	0.6	40.3	0.2	0.1	42.1	0.7	0.4	58.5	0.1	0.1	81.5	0.5	0.1	16.7	0.1	0.1	48.5
Lens of left eye	8.0	2.7	33.1	1.4	0.0	2.6	1.0	0.4	37.1	0.7	0.0	1.2	1.7	0.4	25.6	0.6	0.2	41.1	1.8	1.3	71.7	0.4	0.2	68.5	0.4	0.1	32.1	0.4	0.0	7.0
Right cheek	9.8	1.6	16.8	0.6	0.2	27.5	9.7	1.0	10.1	2.8	0.1	4.9	9.4	3.8	40.8	4.1	1.5	36.9	9.8	6.2	63.4	4.9	3.0	60.5	7.7	2.6	33.5	3.0	0.8	28.2
Nasal cavity	6.8	1.3	18.6	1.2	0.0	1.2	7.0	0.5	7.6	2.0	0.0	0.5	6.2	2.9	46.5	2.2	1.5	68.8	5.2	1.8	34.1	3.0	1.0	33.9	4.2	2.2	51.6	2.9	1.4	49.0
Nasopharyngeal mucosa	7.5	1.4	18.5	3.9	0.3	8.6	8.3	2.1	24.9	3.6	1.5	41.4	8.8	1.5	17.6	2.5	0.6	25.5	5.9	1.7	28.8	2.1	0.5	25.0	1.4	0.8	54.3	0.0	0.0	0.1
Right parotid	10.6	4.2	39.7	4.7	0.6	12.9	8.8	4.0	45.3	5.5	0.3	6.2	8.6	4.8	56.4	4.5	3.3	72.6	7.3	3.1	42.0	4.9	1.0	20.7	5.1	3.1	61.0	1.4	0.7	47.9
Left parotid	11.1	3.6	32.7	2.2	0.5	22.0	9.3	1.5	16.1	7.0	3.1	44.3	11.7	0.3	2.8	3.2	1.2	38.7	6.2	3.2	51.1	4.3	1.2	28.0	5.5	3.2	58.4	1.1	0.6	49.8
Right ramus	8.7	2.1	24.4	3.1	0.5	17.0	7.3	0.2	3.0	3.5	0.6	16.4	6.2	0.2	3.0	4.0	1.1	27.9	5.5	0.6	11.4	2.6	0.2	8.5	2.5	0.8	32.0	0.7	0.3	47.4
Left ramus	8.0	1.4	17.4	2.4	1.0	40.8	8.9	3.9	44.1	3.5	0.1	4.0	6.5	1.6	25.2	3.2	0.1	1.8	4.9	0.1	1.2	2.7	1.9	67.9	1.1	0.1	8.1	1.8	0.2	8.3
Tongue	7.7	0.4	4.5	1.8	0.8	47.1	9.0	3.5	39.3	2.8	0.4	13.2	6.7	0.1	1.5	2.8	0.2	6.1	4.8	0.6	12.5	3.9	1.1	29.2	5.0	0.0	0.8	1.1	0.5	45.0
Center cervical spine	5.3	1.0	18.5	2.6	0.0	0.3	6.1	0.0	0.1	3.0	0.1	3.6	5.1	1.6	30.5	2.6	1.3	51.0	2.8	1.6	57.7	1.1	0.1	10.6	0.6	0.5	79.6	0.7	0.4	50.6
Left back of neck	5.8	0.7	11.4	2.5	0.5	20.0	5.6	2.2	39.2	4.0	0.3	8.1	4.8	2.8	56.8	2.3	0.4	17.4	2.3	0.6	27.5	1.2	0.1	5.8	1.4	0.9	66.2	1.1	0.4	40.1
Right mandibular body	7.8	2.5	31.7	1.7	0.7	38.8	6.3	2.6	41.5	2.9	1.4	49.1	6.7	5.0	74.5	2.1	0.5	21.7	5.0	0.9	18.9	3.0	0.9	29.7	2.2	0.7	30.0	0.8	0.2	21.2
Left mandibular body	6.9	1.6	23.7	3.0	0.6	20.1	6.8	0.7	10.3	2.5	0.8	31.6	6.9	2.4	34.3	2.3	1.0	41.9	4.2	1.6	37.7	3.4	0.9	25.5	2.2	0.8	37.0	1.0	0.4	40.7
Right submandibular gland	9.7	1.7	17.4	2.3	0.8	33.4	7.9	1.7	21.9	4.0	1.5	36.6	10.0	2.5	24.7	2.1	0.8	36.6	8.8	0.8	9.0	2.4	0.7	28.3	1.9	1.0	50.3	0.0	0.0	10.0
Left submandibular gland	9.1	2.1	23.0	3.2	0.5	16.9	6.8	0.2	2.2	3.8	0.1	1.9	7.7	5.3	68.8	3.0	0.1	2.6	5.6	1.5	27.6	3.0	0.7	23.9	1.6	0.1	7.7	0.6	0.1	9.8
Left sublingual gland	7.9	1.0	12.6	2.3	0.0	1.6	8.0	0.1	0.7	3.7	1.3	34.0	9.2	1.0	10.4	2.1	0.5	23.4	6.8	1.5	21.9	2.4	0.4	18.1	1.7	1.3	77.7	0.0	0.0	10.0
Right sublingual gland	9.3	1.6	16.8	2.6	0.1	2.3	7.1	1.2	16.2	3.7	0.6	16.8	8.3	2.8	34.1	2.4	0.9	37.5	6.0	1.7	28.7	2.5	0.6	25.2	1.5	0.1	5.0	0.5	0.0	8.4
Midline thyroid	2.0	0.4	20.7	0.6	0.1	17.6	3.7	0.9	23.5	0.7	0.1	8.6	1.6	0.1	2.9	1.2	0.8	69.2	1.3	0.9	69.0	0.5	0.4	72.7	0.7	0.1	12.2	0.2	0.1	84.7
Thyroid surface—left	2.7	1.8	66.5	0.6	0.0	6.9	1.7	1.0	60.1	0.5	0.2	41.8	1.4	0.0	0.1	0.4	0.2	48.0	1.2	0.2	15.9	0.3	0.0	7.0	0.1	0.1	75.0	0.1	0.0	22.2
Esophagus	0.9	0.2	20.2	0.2	0.1	28.3	0.9	0.3	36.3	0.3	0.0	10.1	0.8	0.2	22.0	0.3	0.0	4.6	0.5	0.1	18.0	0.2	0.2	87.7	0.1	0.1	81.5	0.0	0.0	37.5
Trachea	2.1	0.5	22.4	0.7	0.2	33.6	2.2	0.8	37.0	0.7	0.2	24.3	1.5	0.2	16.1	0.9	0.3	30.7	1.3	0.8	60.2	0.2	0.1	56.8	0.1	0.1	67.8	0.1	0.0	52.9
Spinal canal	1.1	0.2	17.3	0.3	0.0	3.9	1.1	0.7	63.0	0.5	0.0	8.9	1.0	0.3	32.4	0.4	0.1	20.6	0.3	0.0	0.9	0.3	0.2	55.8	0.1	0.1	62.2	0.0	0.0	33.2

	60 × 60 Right maxillary molar A			60 × 60 Right maxillary molar B			60 × 60 Right mandibular molar A			60 × 60 Right mandibular molar B			40 × 40 Anterior maxilla A			40 × 40 Anterior maxilla B			40 × 40 Right maxillary molar A			40 × 40 Right maxillary molar B			40 × 40 Right mandibular molar A			40 × 40 Right mandibular molar B		
	Avg	SD	Var	Avg	SD	Var	Avg	SD	Var	Avg	SD	Var	Avg	SD	Var	Avg	SD	Var	Avg	SD	Var	Avg	SD	Var	Avg	Var	Var	Avg	SD	Var
Calvarium anterior	0.1	0.1	87.2	0.2	0.1	74.7	0.3	0.1	34.9	0.1	0.1	43.3	0.1	0.0	58.3	0.0	0.0	90.0	0.1	0.0	87.6	0.0	0.0	15.2	0.0	0.0	80.2	0.0	0.0	30.0
Calvarium left	0.1	0.1	33.6	0.2	0.0	18.1	0.2	0.1	26.6	0.1	0.0	69.4	0.1	0.1	56.4	0.1	0.1	61.4	0.1	0.1	64.2	0.0	0.0	39.9	0.0	0.0	58.8	0.0	0.0	24.8
Calvarium posterior	0.0	0.0	83.8	0.0	0.0	23.5	0.2	0.1	25.9	0.1	0.0	35.7	0.1	0.0	27.0	0.1	0.1	89.1	0.1	0.1	69.9	0.0	0.0	2.2	0.1	0.1	71.4	0.0	0.0	71.6
Midbrain	0.4	0.2	49.7	0.5	0.1	27.1	0.5	0.0	2.5	0.1	0.1	87.9	0.0	0.0	31.2	0.1	0.1	92.1	0.2	0.1	32.5	0.3	0.1	31.7	0.5	0.4	80.6	0.0	0.0	70.0
Pituitary	1.1	0.0	3.8	1.0	0.9	88.0	0.5	0.4	71.8	0.8	0.7	83.6	0.6	0.2	24.7	0.7	0.7	99.2	0.2	0.1	59.8	0.4	0.3	73.9	0.5	0.2	40.1	0.0	0.0	65.7

(*continued on next page*)

Table V. Continued

	60 × 60 Right maxillary molar A			60 × 60 Right maxillary molar B			60 × 60 Right mandibular molar A			60 × 60 Right mandibular molar B			40 × 40 Anterior maxilla A			40 × 40 Anterior maxilla B			40 × 40 Right maxillary molar A			40 × 40 Right maxillary molar B			40 × 40 Right mandibular molar A			40 × 40 Right mandibular molar B		
	Avg	SD	Var	Avg	SD	Var	Avg	SD	Var	Avg	SD	Var	Avg	SD	Var	Avg	SD	Var	Avg	SD	Var	Avg	SD	Var	Avg	Var	Var	Avg	SD	Var
Right orbit	1.2	0.8	61.4	0.7	0.1	16.9	0.8	0.5	60.8	1.3	0.9	69.5	0.1	0.0	21.9	0.0	0.0	90.0	0.5	0.4	75.6	0.5	0.1	13.9	0.5	0.2	47.4	0.0	0.0	30.0
Left orbit	1.0	0.7	69.7	0.1	0.0	8.3	0.9	0.2	25.0	0.5	0.3	67.9	0.0	0.0	1.0	0.0	0.0	3.1	0.6	0.5	83.3	0.3	0.2	56.2	0.0	0.0	70.0	0.3	0.2	72.8
Lens of right eye	0.6	0.1	10.8	0.2	0.1	49.8	0.7	0.2	22.0	0.2	0.2	82.7	0.7	0.4	61.4	0.1	0.0	36.1	0.2	0.1	75.9	0.1	0.1	90.0	0.5	0.2	39.6	0.3	0.2	67.6
Lens of left eye	0.7	0.2	27.8	0.1	0.0	14.3	1.2	0.4	31.0	0.1	0.1	71.3	0.6	0.3	58.0	0.2	0.1	56.3	0.2	0.1	72.5	0.0	0.0	86.5	0.4	0.2	53.2	0.1	0.1	78.1
Right cheek	4.6	1.4	29.7	0.8	0.3	38.3	8.6	6.0	69.3	1.4	1.0	73.3	7.4	0.5	6.4	4.7	0.5	10.4	3.3	0.7	21.9	2.7	0.5	17.7	4.7	2.2	47.2	0.6	0.4	66.4
Nasal cavity	3.8	3.0	78.9	0.3	0.1	34.3	5.7	1.7	29.4	0.4	0.2	45.9	7.3	4.8	65.0	2.1	1.6	76.0	4.0	3.2	78.9	0.8	0.7	87.7	3.7	1.2	32.6	1.0	0.7	74.5
Nasopharyngeal mucosa	5.5	1.3	23.4	2.6	0.5	17.4	3.9	0.3	7.0	1.8	1.0	58.9	1.7	1.6	93.8	0.8	0.2	29.2	0.9	0.5	53.1	0.9	0.4	49.5	1.5	0.3	20.8	1.6	0.5	31.8
Right parotid	10.8	4.2	39.0	9.3	0.3	3.4	6.6	0.5	7.3	2.6	1.8	67.1	6.1	1.1	18.1	2.2	1.7	75.5	5.8	5.7	98.5	3.9	2.7	70.0	2.5	1.2	48.2	3.0	1.0	32.0
Left parotid	2.8	1.1	38.4	3.5	0.2	6.0	4.1	1.3	32.7	5.3	2.5	46.7	4.6	2.5	53.5	2.2	0.6	27.2	0.8	0.7	95.5	3.9	1.3	34.7	2.7	0.9	33.5	0.0	0.0	40.0
Right ramus	3.2	0.8	24.6	4.9	3.3	67.3	2.5	1.8	71.1	3.9	0.7	17.8	1.3	0.7	55.0	1.3	0.6	47.8	2.1	1.9	91.4	1.7	0.3	17.0	1.9	1.1	54.0	2.0	0.2	10.3
Left ramus	3.8	1.1	28.7	2.5	1.6	65.4	3.3	2.5	75.8	0.8	0.1	9.7	1.1	0.7	66.5	0.2	0.2	79.7	1.6	1.1	67.8	0.4	0.2	42.3	1.4	0.3	19.0	1.9	1.8	91.6
Tongue	3.1	0.0	0.3	4.5	1.0	21.1	5.1	0.2	3.3	2.7	0.0	1.1	1.6	0.1	5.1	0.9	0.4	42.5	0.5	0.2	36.0	2.4	1.2	49.2	5.3	0.9	17.1	0.0	0.0	77.8
Center cervical spine	1.8	0.5	25.7	1.4	0.3	24.4	1.7	0.3	15.1	0.9	0.4	39.3	1.3	0.8	61.8	1.5	0.3	20.7	1.4	1.0	74.9	1.6	1.2	75.6	1.7	1.2	66.4	0.8	0.6	75.0
Left back of neck	1.2	0.4	32.2	1.7	1.4	83.8	2.5	1.0	41.9	1.3	0.6	46.0	1.1	0.9	80.9	1.2	0.4	36.2	0.0	0.0	65.1	1.6	0.7	42.1	1.4	1.2	85.7	1.0	0.8	77.9
Right mandibular body	6.9	1.4	19.8	5.8	3.6	62.0	9.4	1.2	13.2	3.9	1.4	36.1	3.1	1.3	41.1	0.2	0.1	56.9	7.8	6.8	86.6	2.8	1.2	41.8	2.5	2.1	82.5	1.8	1.4	74.2
Left mandibular body	5.5	2.9	51.7	2.0	1.0	50.9	2.2	1.7	75.1	1.8	0.5	25.9	0.6	0.3	53.3	1.3	0.5	33.6	2.6	1.2	46.9	1.8	0.4	21.2	2.5	1.1	42.6	1.9	1.3	66.2
Right submandibular gland	9.9	4.3	43.0	4.6	2.4	52.4	9.3	5.0	53.7	4.8	1.3	27.4	0.7	0.3	47.9	1.8	1.4	76.8	1.6	1.2	75.6	0.6	0.4	67.2	1.5	0.7	46.7	0.7	0.2	22.0
Left submandibular gland	5.0	0.4	7.3	2.5	1.4	57.3	6.2	1.2	19.2	3.0	0.8	26.7	0.7	0.1	17.6	0.3	0.1	39.5	0.8	0.7	85.0	0.5	0.4	78.7	1.5	0.9	61.6	1.0	0.4	40.6
Left sublingual gland	7.4	2.9	38.9	3.3	2.3	70.0	5.9	4.1	69.5	3.6	0.4	11.2	0.8	0.6	71.1	0.3	0.1	33.7	0.6	0.5	75.0	0.7	0.2	27.0	2.2	0.6	25.6	0.7	0.6	79.8
Right sublingual gland	11.1	0.2	1.4	5.0	2.8	54.9	12.3	4.0	32.4	4.3	0.9	21.1	1.3	0.9	72.7	1.6	1.2	72.3	0.0	0.0	70.0	0.3	0.2	65.2	2.0	0.9	44.9	0.7	0.3	46.2
Midline thyroid	0.7	0.2	23.6	0.7	0.5	66.3	1.0	0.1	7.3	0.5	0.1	22.5	0.3	0.1	35.2	0.0	0.0	1.0	0.7	0.6	87.6	0.2	0.1	47.3	0.7	0.2	25.6	0.1	0.0	37.1
Thyroid surface—left	1.2	0.2	19.6	0.4	0.1	21.7	0.8	0.4	54.3	0.2	0.0	2.8	0.3	0.2	44.7	0.0	0.0	37.8	0.3	0.2	68.7	0.1	0.1	73.0	0.7	0.2	27.7	0.1	0.1	48.3
Esophagus	0.3	0.0	12.5	0.1	0.0	43.8	0.2	0.1	46.3	0.2	0.0	2.9	0.1	0.1	95.3	0.0	0.0	33.3	0.2	0.1	57.2	0.1	0.0	31.7	0.1	0.0	36.9	0.1	0.0	31.5
Trachea	0.5	0.1	20.1	0.5	0.2	34.8	0.6	0.3	50.4	0.3	0.2	51.5	0.2	0.2	70.9	0.1	0.0	7.8	0.3	0.2	59.6	0.1	0.1	91.8	0.1	0.1	78.9	0.2	0.1	80.2
Spinal canal	0.3	0.1	27.9	0.1	0.1	67.2	0.3	0.1	25.1	0.3	0.1	37.9	0.0	0.0	29.9	0.0	0.0	18.7	0.1	0.1	85.7	0.3	0.2	82.6	0.1	0.1	85.9	0.2	0.1	26.3

A = 360-degree scans.
B = 180-degree scans,
Avg, average; *SD,* standard deviation; *Var,* variance.

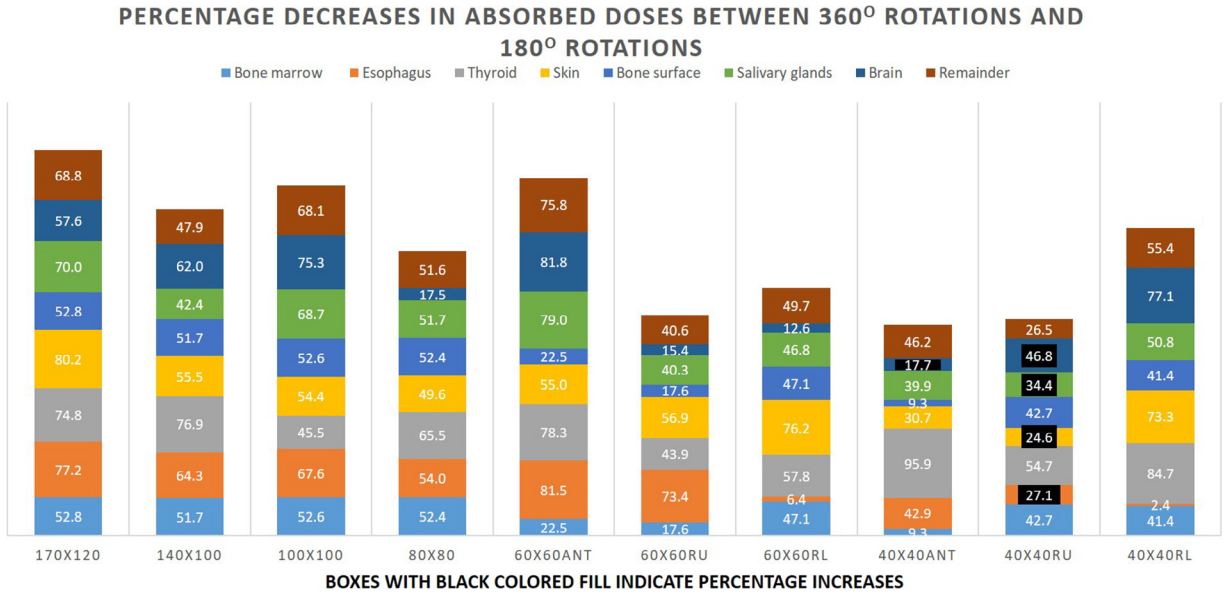

Figure 3. Percentage decreases in absorbed doses in different tissues between 360° rotations and 180° rotations. The boxes with black inserts (all in 40 × 40mm FOVs) represent increased absorbed doses with 180° rotations, while all other boxes represent decreased absorbed doses with 180° rotations. *ANT: anterior maxilla; RU: right maxillary molar; RL: right mandibular molar*

360-degree scans ranged from 74.2 μSv for the right maxillary molar area of the 40 × 40 FOV scans to 436.9 μSv for the 170 × 120 FOV scans. The EDm for 180-degree scans ranged from 30.5 μSv for the anterior maxilla area of the 60 × 60 FOV scans to 176.2 μSv for the 140 × 100 FOV scans. EDm values were lower for 180-degree scans than for 360-degree scans across all FOVs, ranging from a 113.9% decrease for the anterior maxilla area of the 60 × 60 FOV scans to a 16.0% decrease for the right maxillary molar area of the 40 × 40 FOV scans (Table VII); the differences were statistically significant ($P < .01$) for all except the right maxillary molar area of the 40 × 40 FOV protocol.

Comparison of EDm between FOVs

Most phantom-measured effective doses (EDm) were significantly higher ($P < .01$) in larger FOVs (170 × 120; 140 × 100; 100 × 100; and 80 × 80) relative to the smaller FOVs (60 × 60 and 40 × 40) (see Tables VI and VIII). In the 360-degree scans, the EDm values decreased in every comparison of larger to smaller FOVs. The greatest effective dose percentage difference between FOVs in the 360-degree scans, a decrease of 112.4%, was in the right maxillary molar area between the 60 × 60 FOV and 40 × 40 FOV scans (see Table VIII). For the 180-degree scan protocols, the EDm was generally higher in the larger FOVs with 2 exceptions. The EDm for the 170 × 120 FOV scans was 22.2% smaller than for the 140 × 100 FOV scans, and the EDm in the anterior maxilla area of the 60 × 60 FOV scans was 51.6% smaller than in the 40 × 40 FOV scans (see Table VIII).

Comparison of EDm and EDd

The dosimetry-derived EDm values and the EDd values calculated from the DAP for different FOVs and scan protocols are shown in Table VI. The range of EDm values for 360-degree scans extended from 74.2 μSv for the right maxillary molar area of the 40 × 40 FOV scans to 436.9 μSv for the 170 × 120 FOV protocol, as listed above. For the 360-degree scans, the EDd values ranged from 79.8 μSv for the anterior maxilla area of the 40 × 40 FOV scans and right maxillary and right mandibular 40 × 40 scans to 508.0 μSv for 170 × 120 FOV scans. For the 180-degree protocol, EDm was smallest in the anterior maxilla area of the 60 × 60 FOV scans (30.5 μSv) and greatest for the 140 × 100 FOV scans (176.2 μSv), as mentioned in the previous section. EDd ranged from 41.0 μSv for the 3 areas in the 40 × 40 FOV scans to 261.8 μSv for the 170 × 120 FOV scans. The percentage difference between EDm and EDd in the 360-degree scans was lowest (2.1%) for the 80 × 80 FOV and greatest (47.1%) for the right maxillary molar area of the 60 × 60 FOV scans. For 180-degree protocols the percentage difference was lowest (0.1%) for right mandibular molar area of the 40 × 40 FOV scans and highest (93.4%) for the anterior maxilla region in the 60 × 60 FOV scans (Table IX).The differences between EDm and EDd values were highly variable and unpredictable, as shown in Table IX.

Comparison of LOE doses for various protocols

Measured doses to the LOE are shown in Table VI. The dose to the LOE was highest for the 360-degree

Table VI. Contributions of individual tissues to the effective dose based on OSL measurements (EDm), the effective dose calculated from DAP (EDd), and the lens of the eye dose (LOED)

	170 × 120 A	*170 × 120 B*	*140 × 100 A*	*140 × 100 B*	*100 × 100 A*	*100 × 100 B*	*80 × 80 A*	*80 × 80 B*	*60 × 60 Ant max A*	*60 × 60 Ant max B*	*60 × 60 R Max molar A*	*60 × 60 R Max molar B*	*60 × 60 R Man molar A*	*60 × 60 R Man molar B*	*40 × 40 Ant max A*	*40 × 40 Ant max B*	*40 × 40 R Max molar A*	*40 × 40 R Max molar B*	*40 × 40 R Man molar A*	*40 × 40 R Man molar B*
Bone marrow	43.9	20.7	41.2	19.9	36.0	17.1	23.7	11.3	7.2	5.6	16.1	13.3	16.8	8.9	8.9	8.1	12.1	6.9	11.0	6.4
Esophagus	3.5	0.8	3.6	1.3	3.3	1.1	1.9	0.9	0.6	0.1	1.4	0.4	0.9	0.8	0.2	0.1	0.3	0.5	0.3	0.3
Thyroid	92.6	23.3	107.1	24.8	59.8	32.6	50.0	17.2	13.9	3.0	37.9	21.3	36.5	15.4	13.0	0.5	13.6	6.1	27.0	4.1
Skin	3.9	0.8	3.8	1.7	3.6	1.6	3.0	1.5	2.3	1.0	1.5	0.6	2.8	0.7	2.1	1.5	0.8	1.1	1.5	0.4
Bone surface	11.8	5.6	11.1	5.4	9.7	4.6	6.4	3.0	1.9	1.5	4.3	3.6	4.5	2.4	2.4	2.2	11.8	5.6	3.0	1.7
Salivary glands	96.1	28.9	80.0	46.1	92.5	29.0	67.7	32.7	28.8	6.1	78.5	46.8	73.7	39.2	23.5	14.1	15.9	24.3	20.5	10.1
Brain	29.6	12.6	13.6	5.2	18.6	4.6	3.7	3.1	6.9	1.3	6.1	5.2	4.6	4.0	2.1	2.6	1.5	2.9	3.6	0.8
Remainder	155.6	48.5	138.0	71.7	151.0	48.2	109.4	53.0	49.7	12.0	118.9	70.6	113.6	57.3	42.1	22.7	26.8	19.5	38.7	17.2
Effective dose (EDm)	436.9	141.0*	398.5	176.2*	374.5	138.7*	265.9	122.7*	111.1	30.5*	264.6	161.6*	253.3	128.5*	94.4	51.7*	74.2	63.2	105.3	41.0*
ED Calculated from DAP (EDd)	508.0	261.8	429.8	220.6	361.4	186.4	260.4	133.8	163.7	84.0	163.7	84.0	163.7	84.0	79.8	41.0	79.8	41.0	79.8	41.0
Lens of the eye dose (LOED)	8524.5	1241.4*	4190.5	1986.7*	3580.9	1286.2*	816.0	489.6*	2475.0	1155.6*	844.7	302.8*	896.2	301.4*	330.8	68.9*	369.9	215.0*	331.1	168.3*

A = 360-degree scans.
B = 180-degree degree scans.
EDm: Effective dose (μSv): Product of equivalent dose and 2007 ICRP tissue weighting factors (Note EDm is the sum of values of individual tissues).
EDd: Effective dose (μSv) calculated from DAP as (0.001453)(kV) + (0.0118)(PKA), where kV = tube voltage and PKA = displayed DAP.
LOED: Lens of the eye dose is the absorbed dose calculated as the summed ipsilateral lens of the eye dose and orbital dose. This dose does not contribute to the effective dose.
Ant, anterior; *Man,* mandible; *Max,* maxilla; *R,* right.
*Differences between 360-degree and 180-degree scan doses significant at $P < .01$.

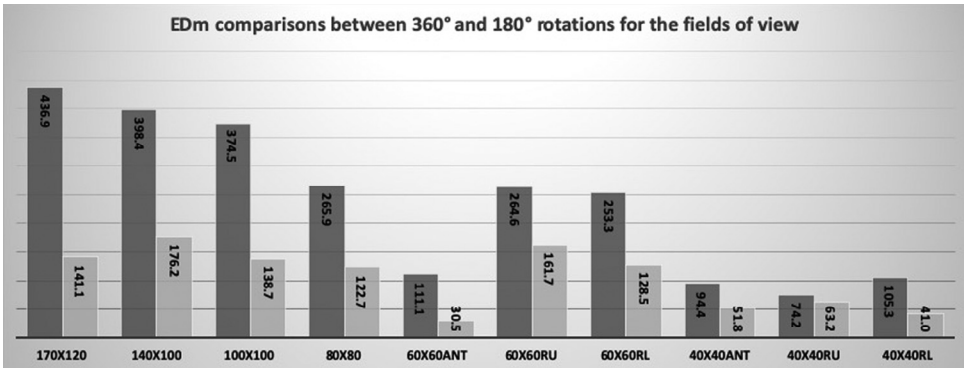

Figure 4. Effective doses (μSv) calculated from direct OSL measurements. Effective dose comparisons between 360° rotations (dark grey) and 180° rotations (light grey) for different fields of view. *ANT: anterior maxilla; RU: right maxillary molar; RL: right mandibular molar*

protocol in the 170 × 120 FOV scans (8524.5 μSv), and for the 180-degree protocol in the 140 × 100 FOV scans (1986.7 μSv). The LOE dose was lowest for anterior maxilla region in the 40 × 40 FOV scans for both 360-degree (330.8 μSv) and 180-degree (68.9 μSv) scans. The EDm values for the LOE were smaller in all 180-degree scans compared with the 360-degree scans, and the differences were significant for the 170 × 120, 140 × 100, 100 × 100, and the anterior maxilla are of the 60 × 60 FOV scans (see Table VI). The greatest percentage difference between the 360-degree and 180-degree protocols was for the 170 × 120 FOV scan (149.2 %) and the smallest percentage difference for 80 × 80 FOV (50.0%), as shown in Table VII.

DISCUSSION

Effective dose is a mathematical construct intended for use in calculating radiation limits to workers and the public for protection from radiation. Effective dose is not a radiation dose per person but, rather, is a computed number calculated for a reference person and not for a specific individual.[25] This study measured the differences in absorbed doses (see Table V) and calculated the differences in EDs among CBCT acquisitions using different FOVs with 360-degree versus 180-degree rotation arcs (see Table VI). ADs, EDs, and LOE doses were substantially lower in the 180-degree scans compared with the 360-degree scans across all FOVs (see Tables VI, VII, and VIII). The findings of this investigation reaffirm the results of prior studies on varying FOV scans using different rotation angles.[14,15] The present study also showed that EDd values derived from machine-displayed DAP values have considerable variation from the measured EDm derived from phantom dosimetry (see Table IX).

ADs were substantially lower with 180-degree rotation arcs compared with 360-degree rotation arcs at almost every measured site but were higher for some tissues in a few protocols (see Table V). AD is an averaged dose, hence the doses recorded in the different dosimeters will affect its value. The dosimeters outside the FOV showed large variability in dose because they were distant from the primary beam and sparingly recorded scattered radiation. Other studies have recommended using large numbers of dosimeters to overcome such errors.[26] However, this was beyond the capabilities of the present study. Also, dosimeters located peripherally tend to have small positional differences among scans, as opposed to the dosimeters placed within internal organs.[2] This may account for the variations in skin and thyroid doses in our study. The study by Ludlow has shown that a 10-degree rotation in phantom position with respect to the Frankfurt horizontal plane moves the position of the superficial thyroid gland into or out of the FOV of the primary beam and produces a 92% difference in the dose to thyroid.[27]

EDs were significantly lower for small FOVs (40 × 40 and 60 × 60) than for large FOVs (80 × 80; 100 × 100; 140 × 100; and 170 × 120) for both 360-degree and 180-degree arcs (see Tables VI, VII, and VIII). ED percentage differences in full-rotation scans were as high as 112.4% (for 60 × 60 FOVs relative to the corresponding 40 × 40 FOVs), although this could have been slightly overestimated (see Table VIII). Loubele et al. suggested that maxillary FOV doses are larger than mandibular FOV doses because dense bone in the mandible attenuates more x-rays compared with the maxilla.[1] The half-rotation scan ED for the 170 × 120 FOV was, in fact, 22.2% lower than for the smaller 140 × 100 FOV, and the 60 × 60 anterior maxilla FOV dose was 51.6% lower than the smaller 40 × 40 FOV dose (see Table VIII). The reasons for these variations may be attributed to errors in the calculations of the ADs for the corresponding tissues in the FOVs, as discussed above. Studies have shown that differences in EDs for similar FOVs with different CBCT

Table VII. Percentage differences in effective doses calculated from dosimeter measurements (EDm) between 360-degree and 180-degree scans for different fields of view (FOV), and percentage decreases in absorbed doses to the lens of the eye between 360-degree and 180-degree scans for different fields of view

	170 × 120	*140 × 100*	*100 × 100*	*80 × 80*	*60 × 60 Anterior Maxilla*	*60 × 60 Right maxillary molar*	*60 × 60 Right mandibular molar*	*40 × 40 Anterior Maxilla*	*40 × 40 Right maxillary molar*	*40 × 40 Right mandibular molar*
Effective dose percentage reduction from 360-degree to 180-degree scans	102.5	77.5	92.0	73.8	113.9	48.4	65.5	58.5	16.0	88.0
Lens of the eye percentage reduction from 360-degree to 180-degree scans†	149.3	71.5	94.4	50.1	72.8	94.5	99.4	131.1	53.1	65.3

*EDm was significantly lower ($P < .01$) for 180-degree scans for every FOV except right maxillary anterior 40 × 40.
†Absorbed dose to lens of the eye was significantly lower ($P < .01$) for 180-degree scans at every FOV.

Table VIII. Percentage differences in effective dose calculated from dosimetry (EDm) between different fields of view (FOVs) for 360-degree and 180-degree scans

	170 × 120 to 140 × 100	*140 × 100 to 100 × 100*	*100 × 100 to 80 × 80*	*80 × 80 to 60 × 60 Anterior maxilla*	*60 × 60 to 40 × 40 Anterior maxilla*	*60 × 60 to 40 × 40 Right upper molar*	*60 × 60 to 40 × 40 Right lower molar*
360-degree rotation	9.2^{+}	6.2^{+}	33.9^{+}	82.1^{+}	16.3^{+}	112.4^{+}	82.5^{+}
180-degree rotation	22.2^{-}	23.8^{+}	12.2^{+}	120.4^{+}	51.6^{-}	87.5^{+}	103.2^{+}

FOV in mm × mm.
+Indicates EDm was significantly higher for large FOV scan.$^{-}$Indicates EDm was significantly lower for large FOV scan.

Table IX. Percentage differences between effective dose calculated from dosimetry (EDm) and effective dose calculated from dose area product (DAP) (EDd)

	170 × 120	*140 × 100*	*100 × 100*	*80 × 80*	*60 × 60 Anterior maxilla*	*60 × 60 Right maxillary molar*	*60 × 60 Right mandibular molar*	*40 × 40 Anterior maxilla*	*40 × 40 Right maxillary molar*	*40 × 40 Right mandibular molar*
Percentage difference (360-degree scans)	15.0^{-}	7.6^{-}	3.6^{+}	2.1^{+}	38.3^{-}	47.1^{+}	43.0^{+}	16.8^{+}	7.3^{-}	27.6^{+}
Percentage difference (180-degree scans)	60.0^{-}	22.4^{-}	29.3^{-}	8.7^{-}	93.4^{-}	63.2^{+}	41.9^{+}	23.1^{+}	42.6^{+}	0.1^{+}

Field of view (FOV) in mm × mm.
Values in percentages.
+Indicates EDm was significantly higher than EDd ($P < .01$). $^{-}$Indicates EDm was significantly lower than EDd ($P < .01$).

units can be a function of units can be a function of milliamp seconds (mAs) and are determined by the height, diameter, and position of the FOV.[2,14] Previous investigations have revealed that a 16 × 4 cm FOV for the mandible reduces dose by 24% to 46% compared with 14 × 5 cm or 16 × 6 cm FOVs. In contrast to our study and other previous studies,[14] Ludlow et al. did not find statistically significant differences in EDs between large and medium FOV scans.[3]

There was a greater than 50% dose reduction from 360-degree rotation scans to 180-degree rotation scans for large FOV acquisitions and some small FOV scans and close to, but less than, 50% for the remaining small FOV acquisitions (40 × 40 and 60 × 60 right maxillary molar scans). Although the results for large FOVs are not consistent with those of some of the previous studies, the results for small FOV scans are consistent.[14,15] The reduced ED is closely related to the reduced scan time from 17.5 seconds in the 360-degree scan to 9 seconds in the 180-degree scan. Thus, the mAs is nearly half of that in a 360-degree scan.

Accuitomo units provide different rotation settings, including the initial position of the tube head and rotation arc of the tube. For half-rotation scans the tube can rotate around either the anterior or the posterior half of the patient. Because more of the radiosensitive organs in the head and neck region are located in the anterior half, most studies have employed posterior rotation of the tube.[15,28] Therefore, we employed posterior rotation in our project. Zhang et al. manipulated the initial positions of the tube and found small variations in EDs.[28]

A critical factor to consider when half-rotation scans are used is degraded image quality as well as the potential diminished diagnostic efficacy resulting from reduced scan time and number of basis projections. However, ex vivo studies on detection of external root resorption, periapical bone loss, periapical lesions, evaluation of mini-implant sites, simulated condylar degenerative changes, and inferior alveolar canal mapping have shown comparable diagnostic outcomes for 180-degree scans and 360-degree scans.[16-20,29,30] Relative diagnostic efficacies have not been prospectively studied in vivo; such research is presently nearing completion. Thus, although image quality may be reduced because of increased noise and artifacts from the lower mAs setting for half-rotation scans, diagnostic efficacy appears to be comparable with that of 360-degree scans.

The use of DAP to determine patient doses and EDs has been debated vigorously in the literature.[3,22] Although it is easy to obtain DAP from machine displays or calculate it from the DAP meter, this does not take into consideration the differences in the tissues exposed. For example, DAP for the anterior maxilla

and the posterior mandible in a 40 × 40 view would be the same, whereas the ED values calculated from measured ADs would be substantially different. Nevertheless, many authors have used conversion coefficients to calculate ED from DAP.[22,24] In our study, percentage differences between DAP-based EDd and phantom dosimetry-based EDm for large FOV 360-degree scans were in the range of 2% to 15%, with EDm from phantom dosimetry being lower than EDd for the 170 × 120 and 140 × 100 FOV scans but higher than EDd for the 100 × 100 and 80 × 80 scans. For smaller FOVs, EDm values from phantom dosimetry were higher than EDd values for all FOVs except the 40 × 40 right maxillary molar area and 60 × 60 anterior maxilla region. The percentage differences for the smaller FOVs ranged from 7.3% to 47.1%.

The percentage differences for 180-degree scans varied widely. The smallest percentage difference was seen for the right mandibular molar area in the 40 × 40 FOV scans (0.1%), whereas the greatest difference was recorded for the anterior maxilla area in the 60 × 60 FOV scans (93.4%). Such variations for EDd calculated from DAP have also been seen previously.[22,31] Present DAP values in CBCT instruments can vary greatly from the directly measured absorbed doses, but they do not appear to have the same validity for CBCT exposures as they do for MDCT exposures, making their use in CBCT imaging questionable. However, we caution that EDm calculated from phantom dosimetry can also have variations as a result of subtle positional differences of the phantom and superficially placed dosimeters.

The risk of radiation cataractogenesis, a tissue reaction and not a stochastic effect, to the LOE has attracted considerable attention recently as a result of the unclear relationship between radiation dose and cataract formation.[32] The ICRP had considered the threshold for cataractogenesis to be an LOE AD of 500 mGy. Threshold doses for LOE recently were lowered to 30 mSv in the ICRP publication No. 118.[32] This change has generated considerable debate in the health physics community. Doses for LOE in our study were far lower than either of these threshold values. The LOE doses were considerably lower with smaller FOVs, consistent with a trend that was noted by Pauwels et al. in their study with the Accuitomo scanner and LOE doses.[14]

Our study had some limitations. We used a phantom that had been modified for previous studies, most notably with the hollowing out of an area approximating the oral cavity and a slot to house rectangular collimating instruments. This likely had relatively small and variable impacts on the scattered radiation with different FOVs. In previous studies, the hollowed slot for housing intraoral detectors created asymmetry in radiation moving through the tissue-equivalent material. Also, we attempted to minimize the issue of dosimeter sensitivity by using multiple exposures for all FOVs. However, the nanoDot dosimeters were read out only once by the microStar reader; thus, there may have been technical errors related to a single read. Multiple readouts for each exposed dosimeter are recommended in such studies.

CONCLUSIONS

Organ absorbed doses, effective doses, and doses to the LOE decreased substantially when CBCT imaging was performed with 180-degree (half-rotation) protocols and smaller FOVs. The calculated EDs from EDm are likely to have variations as a result of errors in dosimeter placements and phantom positioning among the scans. DAP as the basis for measurement of EDd values had considerable variation from EDm values. Although the selection of CBCT acquisition factors continues to have a strong clinical judgment basis, in view of the substantial dose reduction with half-rotation scans and smaller FOVs, we recommend the use of reduced rotation arcs and the smallest FOV commensurate with the diagnostic task, when clinically possible. This is especially true when imaging children and adolescents. Multiple ex vivo laboratory studies showing comparable diagnostic efficacy in clinically relevant situations await verification through in vivo studies. We think it would be in the best interests of patient safety if manufacturers provided such options in their CBCT scanners.

REFERENCES

1. Loubele M, Bogaerts R, Van Dijck E, et al. Comparison between effective radiation dose of CBCT and MSCT scanners for dentomaxillofacial applications. *Eur J Radiol*. 2009;71:461-468.
2. Ludlow JB, Davies-Ludlow LE, Brooks SL, Howerton WB. Dosimetry of 3 CBCT devices for oral and maxillofacial radiology: CB Mercuray, NewTom 3G and i-CAT. *Dentomaxillofac Radiol*. 2006;35:219-226.
3. Ludlow JB, Timothy R, Walker C, et al. Effective dose of dental CBCT—a meta-analysis of published data and additional data for nine CBCT units. *Dentomaxillofac Radiol*. 2015;44:20140197.
4. Brenner DJ, Hall EJ. Computed tomography—an increasing source of radiation exposure. *N Engl J Med*. 2007;357:2277-2284.
5. United Nations Scientific Committee on the Effects of Atomic Radiation (UNSCEAR).Annex B: Uncertainties in risk estimates for radiation-induced cancer, In: Sources, Effects and Risks of Ionizing Radiation. UNSCEAR 2012 Report to the General Assembly, Scientific Annexes. New York: United Nations; 2015; Publication E.16.IX.1.
6. National Council on Radiation Protection and Measurements (NCRP). *Implications of Recent Epidemiologic Studies for the Linear-Nonthreshold Model and Radiation Protection. NCRP Commentary No. 27*. Bethesda, MD: NCRP; 2018.

7. Ludlow JB, Walker C. Assessment of phantom dosimetry and image quality of i-CAT FLX cone beam computed tomography. *Am J Orthod Dentofacial Orthop*. 2013;144:802-817.
8. Goren AD, Prins RD, Dauer LT, et al. Effect of leaded glasses and thyroid shielding on cone beam CT radiation dose in an adult female phantom. *Dentomaxillofac Radiol*. 2013;42:20120260.
9. Rehani MM. Radiological protection in computed tomography and cone beam computed tomography. *Ann ICRP*. 2015;44:229-235.
10. Feragalli B, Rampado O, Abate C, et al. Cone beam computed tomography for dental and maxillofacial imaging: technique improvement and low-dose protocols. *Radiol Med*. 2017;122:581-588.
11. Pauwels R, Silkosessak O, Jacobs R, Bogaerts R, Bosmans H, Panmekiate S. A pragmatic approach to determine the optimal kVp in cone beam CT: balancing contrast-to-noise ratio and radiation dose. *Dentomaxillofac Radiol*. 2014;43:20140059.
12. Pauwels R, Seynaeve L, Henriques JCG, et al. Optimization of dental CBCT exposures through mAs reduction. *Dentomaxillofac Radiol*. 2015;44:20150108.
13. Pauwels R, Araki K, Siewerdsen JH, Thongvigitmanee SS. Technical aspects of dental CBCT: state of the art. *Dentomaxillofac Radiol*. 2015;44:20140224.
14. Pauwels R, Zhang G, Theodorakou C, et al. Effective radiation dose and eye lens dose in dental cone beam CT: effect of field of view and angle of rotation. *Br J Radiol*. 2014;87:20130654.
15. Morant JJ, Salvado M, Casanovas R, Hernandez-Giron I, Velasco E, Calzado A. Validation of a Monte Carlo simulation for dose assessment in dental cone beam CT examinations. *Phys Med*. 2012;28:200-209.
16. Al-Nuaimi N, Patel S, Foschi F, Mannocci F. The detection of simulated periapical lesions in human dry mandibles with cone-beam computed tomography: a dose reduction study. *Int Endod J*. 2016;49:1095-1104.
17. Yadav S, Palo L, Mahdian M, Upadhyay M, Tadinada A. Diagnostic accuracy of 2 cone-beam computed tomography protocols for detecting arthritic changes in temporomandibular joints. *Am J Orthod Dentofacial Orthop*. 2015;147:339-344.
18. Tadinada A, Marczak A, Yadav S. Diagnostic efficacy of a modified low-dose acquisition protocol for the preoperative evaluation of mini-implant sites. *Imaging Sci Dent*. 2017;47:141-147.
19. Librizzi ZT, Tadinada AS, Valiyaparambil JV, Lurie AG, Mallya SM. Cone-beam computed tomography to detect erosions of the temporomandibular joint: effect of field of view and voxel size on diagnostic efficacy and effective dose. *Am J Orthod Dentofacial Orthop*. 2011;140:e25-e30.
20. Tadinada A, Schneider S, Yadav S. Evaluation of the diagnostic efficacy of two cone beam computed tomography protocols in reliably detecting the location of the inferior alveolar nerve canal. *Dentomaxillofac Radiol*. 2017;46:20160389.
21. Thilander-Klang A, Helmrot E. Methods of determining the effective dose in dental radiology. *Radiat Prot Dosimet*. 2010;139:306-309.
22. Shin HS, Nam KC, Park H, Choi HU, Kim HY, Park CS. Effective doses from panoramic radiography and CBCT (cone beam CT) using dose area product (DAP) in dentistry. *Dentomaxillofac Radiol*. 2014;43:20130439.
23. International Commission on Radiological Protection (ICRP). The 2007 Recommendations of the International Commission on Radiological Protection. ICRP Publication 103. *Ann ICRP*. 2007;37:1-332.
24. Batista WO, Navarro MVT, Maia AF. Development of a phantom and a methodology for evaluation of depth kerma and kerma index for dental cone beam computed tomography. *Radiat Prot Dosimet*. 2013;157:543-551.
25. Fisher DR, Fahey FH. Appropriate use of effective dose in radiation protection and risk assessment. *Health Phys*. 2017;113:102-109.
26. Pauwels R, Beinsberger J, Collaert B, et al. Effective dose range for dental cone beam computed tomography scanners. *Eur J Radiol*. 2012;81:267-271.
27. Ludlow JB. Dose and risk in dental diagnostic imaging: with emphasis on dosimetry of CBCT. *Korean J Oral Maxillofac Radiol*. 2009;39:175-184.
28. Zhang G, Marshall N, Bogaerts R, Jacobs R, Bosmans H. Monte Carlo modeling for dose assessment in cone beam CT for oral and maxillofacial applications. *Med Phys*. 2013;40:072103.
29. Durack C, Patel S, Davies J, Wilson R, Mannocci F. Diagnostic accuracy of small volume cone beam computed tomography and intraoral periapical radiography for the detection of simulated external inflammatory root resorption. *Int Endod J*. 2011;44:136-147.
30. Lennon S, Patel S, Foschi F, Wilson R, Davies J, Mannocci F. Diagnostic accuracy of limited volume cone-beam computed tomography in the detection of periapical bone loss: 360 degrees scans versus 180 degrees scans. *Int Endod J*. 2011;44:1118-1127.
31. Kim S, Yoshizumi TT, Toncheva G, Frush DP, Yin FF. Estimation of absorbed doses from paediatric cone-beam CT scans: MOSFET measurements and Monte Carlo simulations. *Radiat Prot Dosimet*. 2010;138:257-263.
32. Stewart FA, Akleyev AV, Hauer-Jensen M, on behalf of ICRP. ICRP statement on tissue reactions and early and late effects of radiation in normal tissues and organs—threshold doses for tissue reactions in a radiation protection context. ICRP publication 118. *Ann ICRP*. 2012;41:1-322.

Reprint requests:

Alan Lurie
Professor and Chair
Section of Oral and Maxillofacial Radiology
University of Connecticut, School of Dental Medicine
263 Farmington Avenue
Farmington
CT 06030-1605
USA.
lurie@uchc.edu